Using randomly distributed charges to create quantum dots

O. Makarovsky,[1,*] A. G. Balanov,[1,2,*] L. Eaves,[1] A. Patanè,[1] R. P. Campion,[1] C. T. Foxon,[1] and R. J. Airey[3]
[1]*School of Physics & Astronomy, University of Nottingham, Nottingham NG7 2RD, United Kingdom*
[2]*Department of Physics, Loughborough University, Loughborough LE11 3TU, United Kingdom*
[3]*Department of Electronic & Electrical Engineering, University of Sheffield, Sheffield S1 3JD, United Kingdom*
(Received 19 October 2009; published 14 January 2010)

Using a combination of modeling and tunneling spectroscopy, we investigate how electrostatic potential fluctuations generated by randomly distributed ionized donors close to a quantum well can produce deep and strongly confined quantum-dot-like potential minima with a rich spectrum of zero-dimensional electronic energy levels. We consider different types of random distribution of donors and how the electronic properties can be controlled and investigated in appropriately designed double barrier resonant tunneling diodes.

DOI: 10.1103/PhysRevB.81.035323 PACS number(s): 73.22.−f, 71.55.Eq, 71.70.Ej, 73.63.Kv

I. INTRODUCTION

A quantum dot (QD) is a nanostructure in which an electron is confined in all three spatial directions. This results in an atomiclike spectrum of discrete energy levels. A confinement potential deep enough to accommodate several widely spaced energy levels[1] can be achieved in semiconductor structures by a variety of techniques including Stranski-Krastanow self-assembly,[1–4] colloidal synthesis,[5,6] nanoscale patterning or etching,[7,8] monolayer fluctuations of thin quantum well layers,[9] or electrostatic confinement in gated submicron transistors with planar or multilayer geometries.[10,11] Recently, we demonstrated an alternative method of QD fabrication, by post-growth annealing of a functional semiconductor device.[12] For a narrow range of annealing conditions, it is possible to diffuse doubly ionized manganese interstitial donors (Mn_i^{2+}) out of a surface layer of ferromagnetic *p*-type $Ga_{1-x}Mn_xAs$ into an underlying layer of undoped GaAs adjacent to a quantum well (QW). The random clustering of Mn_i^{2+} ions modifies the electrostatic potential within the well, giving rise to a small number of deep potential-energy minima, each of which can quantum-confine conduction electrons on a length scale $l_0 \sim 10$ nm. In this paper, we develop a theoretical model to understand how these potential minima are formed and how the characteristic energy level spacing of bound conduction electrons can be adjusted by fine tuning of the semiconductor heterostructure design. We compare the model calculations with our experimental data and also discuss the relevance of our results to previous reports of unexpected "growth-induced" quantum dot potentials.[13–15]

II. SIMULATING THE POTENTIAL GENERATED BY RANDOMLY DISTRIBUTED ELECTRICAL CHARGES

In this section we model the electrostatic potential profile generated by randomly distributed ionized donors in the vicinity of a quantum well. We consider three different distributions shown schematically in Figs. 1(a)–1(c): (i) Mn_i^{2+} donors, which have diffused along the growth axes, *z*, from a layer of ferromagnetic $Ga_{1-x}Mn_xAs$ toward the well; (ii) a uniform and random "charged slab" distribution (three-dimensional doping); and (iii) a single δ layer of donors [two-dimensional (2D) doping] close to the well.

The first distribution corresponds to the experimental situation recently described in Ref. 12. The device is a *p-i-n* double barrier resonant diode (RTD) in which the *p*-type top barrier is $Ga_{1-x}Mn_xAs$ with $x=3\%$; see Fig. 1(d). The $Ga_{1-x}Mn_xAs$ layer is separated from the GaAs/AlAs quantum well by a 10 nm spacer layer of undoped GaAs. When the device is thermally annealed, the Mn_i^{2+} ions diffuse to the top surface layer and also into the GaAs spacer layer. The diffusion of Mn_i^{2+} can be described by a simple one-dimensional model based on Fick's law. In the low-diffusion limit, the mean concentration, *C*, of Mn_i^{2+} at a distance *z* below the (GaMn)As/GaAs interface and after an annealing time, t_A, is given by

$$C(z,t) = C_s erfc\left(\frac{z}{2\sqrt{Dt_A}}\right). \quad (1)$$

Here $C_s \approx 5\times 10^{19}$ cm^{-3} is the concentration of Mn_i^{2+} in the $Ga_{1-x}Mn_xAs$ layer (for $x=3\%$, $\sim 10\%$ of Mn atoms occupy interstitial positions), $D=D_0 \exp(-Q/k_BT_A)$ is the Mn_i^{2+} diffusion coefficient, $D_0=3\times 10^{-4}$ m^2/s, $Q=1.5$ eV is the activation energy[16] and T_A is the annealing temperature.

We simulate numerically the distribution of Mn_i ions for $T_A=150$ °C, neglecting Coulomb interactions between them.

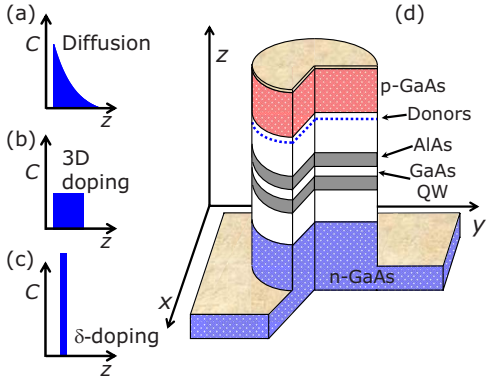

FIG. 1. (Color online) Distributions of positively charged donors close to a QW in a GaAs/AlAs *p-i-n* RTD. (a) Distribution for diffusive charge. (b) A uniform and random "charged slab" distribution. (c) A δ layer of ionized donors.

TABLE I. Average number of Mn_i clusters and corresponding number of Mn_i in each cluster for a mesa of diameter $D=200$ μm.

Average number of Mn_i clusters, N_c	160000	6800	235	7	0.2	0.004	10^{-4}	10^{-6}
Number of Mn_i in each cluster, M	3	4	5	6	7	8	9	10

This is a reasonable approximation since the Mn_i density in the GaAs spacer is relatively low, changing from $\sim 10^{19}$ cm^{-3} at the (GaMn)As interface (i.e., a mean Mn_i separation >5 nm and a Coulomb interaction energy less than Q and $k_B T_A$) to effectively zero at the AlAs/GaAs interface. Our simulated positions of individual Mn_i in the QW plane (x,y) are defined by random numbers corresponding to "white noise" of uniform distribution, with the ion density along the growth axis z given by $C(z,t)$. In this case, the concentration of charge obeys Poissonian statistics and the probability of finding a nanocluster with a number M of Mn_i^{2+} ions is given by $P_M = \langle M \rangle^M e^{-\langle M \rangle}/M!$.[17] Here $\langle M \rangle = CV_C$ is the average number of Mn_i^{2+} donors within a cluster of volume V_C. Table I compares the number of clusters, N_c, with M Mn_i^{2+} ions in each cluster at a distance 8 nm from the (GaMn)As/GaAs interface for $V_C \approx 1000$ nm^3. In an area of 200 μm diameter, one can expect to find a small, but significant, number of clusters of size ~ 10 nm with 6–8 Mn_i^{2+} ions in each of them, and a much larger number with, say, 3–5 ions. Note that this statistical result agrees with numerical simulations of Mn_i diffusion. The simulations involve 3×10^6 Mn_i^{2+} ions occupying a volume of $5 \times 5 \times d$ μm^3, where d is the distance from the (GaMn)As/GaAs interface to the central plane of the QW. Figure 2(a) shows the resulting electronic potential energy $U_{QW}(x,y)$ for $d=20$ nm in the central area $(0.3 \times 0.3$ $\mu m^2)$ of our simulation, over which edge effects can be neglected. The potential-energy contours in Fig. 2(a) reveal a complex landscape. This arises from random spatial variations in the density profile of diffused Mn_i with nanoscale regions ("clusters") extending over ~ 10 nm, where the local density of Mn_i considerably exceeds the mean density at this value of d, typically by a factor of 3–4.

The clusters giving rise to the deepest potential minima contain typically up to ~ 10 randomly placed Mn_i ions and form in the GaAs layer just below the (GaMn)As layer. By solving numerically the 2D Schrödinger equation of an electron in one of the minima using the effective-mass approximation ($m^* = 0.067 m_e$ for conduction electrons in the GaAs QW) as a function of the magnetic field B parallel to the z direction, we obtain the magnetospectrum shown in Fig. 2(d). The rich energy level spectrum resembles the states of the Fock-Darwin model for an electron in a 2D harmonic potential in the presence of a magnetic field.[12,18] It has been shown previously that this model provides a reasonable approximation to the electronic states of circular QDs formed by submicron lithography.[11,19,20]

Figures 2(a)–2(c) show the electronic potential energy $U_{QW}(x,y)$ of the same random distribution of ions for three different values of d. A comparison of the results of numerical simulation summarized in Fig. 2 suggests a way of adjusting the density and typical depth and curvature of the minima in $U_{QW}(x,y)$. For example, by reducing d from 20 to 10 nm, we can increase the number of potential minima and obtain a larger value of the characteristic level spacing.

We have performed 98 simulations of the electrostatic potential induced by different sets of randomly distributed ions and found about 80 simulations with deep (>0.3 eV) potential-energy minima and low-energy contours close to elliptical. Many (>50%) of these dots have approximately circular potentials with energy spectra similar to the Fock-Darwin model. Deviations from exact circular symmetry are evident from the lifting of the orbital degeneracy of the $2p$-like and other excited state levels, see Figs. 2(d)–2(f). However, this splitting is usually smaller than that corresponding to the principal quantum number; hence, in most cases, orbital angular momentum is a "good" quantum num-

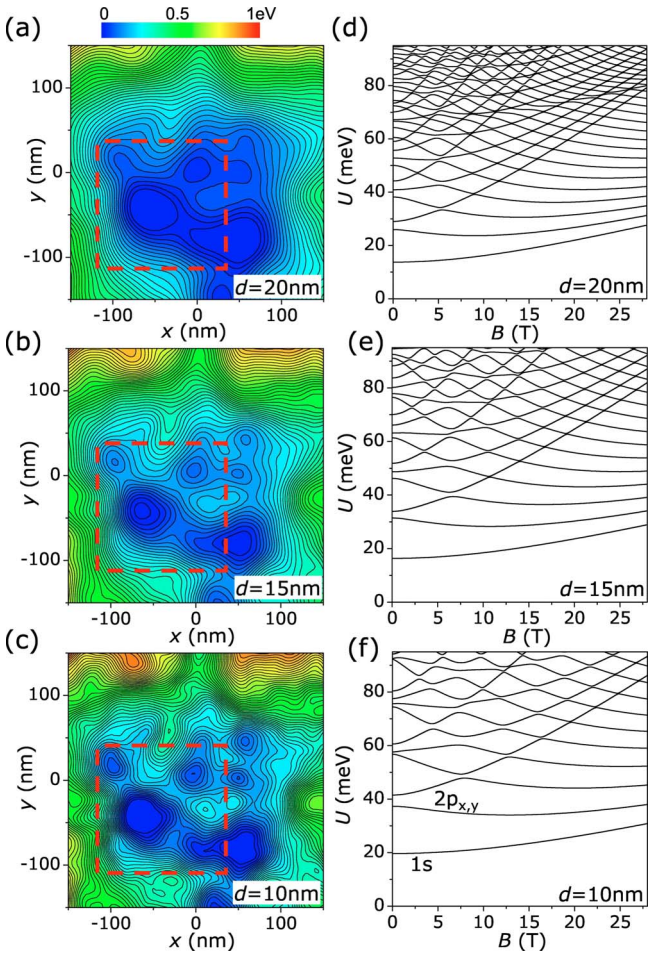

FIG. 2. (Color online) Numerical simulation of the electrostatic potential created by randomly distributed nanoclusters of Mn_i ions for (a) $d=20$ nm, (b) 15 nm, and (c) 10 nm. Parts (d), (e), and (f) represent corresponding Fock-Darwin-type energy spectra of electrons confined in the potential minima in the area indicated by a square. In figure (f), the three lowest energy states at low B are labeled $1s$ and $2p_{x,y}$.

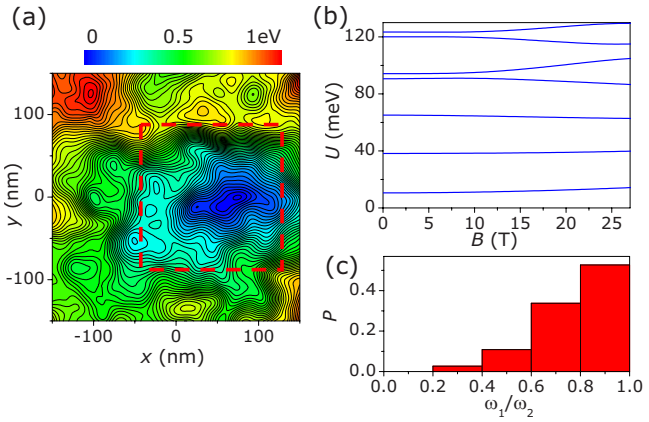

FIG. 3. (Color online) (a) Numerical simulation of the electrostatic potential for an elongated quantum dot. (b) Energy spectra of the QD shown in part (a). (c) Probability to find a QD whose cross-section in the (x,y) plane is approximated by an ellipse with axis ratio ω_2/ω_1 $(\omega_2 \geq \omega_1)$.

ber at moderate values of $B(\geq 5$ T). This behavior is consistent with the homogenous distribution of ions in the xy plane; probabilistically there is no preferred direction in the disposition of the ions. However, four quantum dots out of the 80 obtained from our simulation have a cross-section, which is approximated by elongated elliptical contours with aspect ratio ≤ 0.4. An example of such confining potential and the corresponding energy spectrum are shown in Figs. 3(a) and 3(b). The spectra of the elongated QDs are very different from the Fock-Darwin form. In particular, the splitting due to the lowered symmetry becomes comparable with the level spacing associated with the principal quantum number and the orbital Zeeman splitting of the low-energy excited states is effectively quenched. A statistical analysis of the shapes of the different quantum dots obtained from our simulations is summarized in Fig. 3(c), where we plot the probability P of finding a quantum dot whose low-energy potential contours can be approximated by an ellipse with axis ratio ω_2/ω_1 $(\omega_2 \geq \omega_1)$. Note how P drops rapidly as ω_2/ω_1 decreases from 1.

To understand how different types of random distributions affect the form of the electrostatic potential, we performed additional calculations with a uniform charged slab distribution [Fig. 1(b)] and a single δ layer of double-ionized donors close to a well [Fig. 1(c)]. Similar numerical simulations of the fluctuating electrostatic potential have been reported for quantum wires made from δ-modulation doped heterostructures.[21] Our simulations use the same coordinates x,y of ions as those for the calculations shown in Fig. 2. However, for the case of the slab distribution the ions were uniformly placed along z, over the 10 nm thickness of the slab; for the δ-layer distribution, the z coordinate of ions was fixed. The results summarized in Fig. 4 indicate that the potential generated by the random slab of charge and by the δ layer are qualitatively similar to those obtained for diffused ions distributed along z. Thus, we conclude that the appearance of deep potential minima resulting from clustering of randomly distributed charges in the proximity of a quantum well does not depend significantly on the distribution of ions along z.

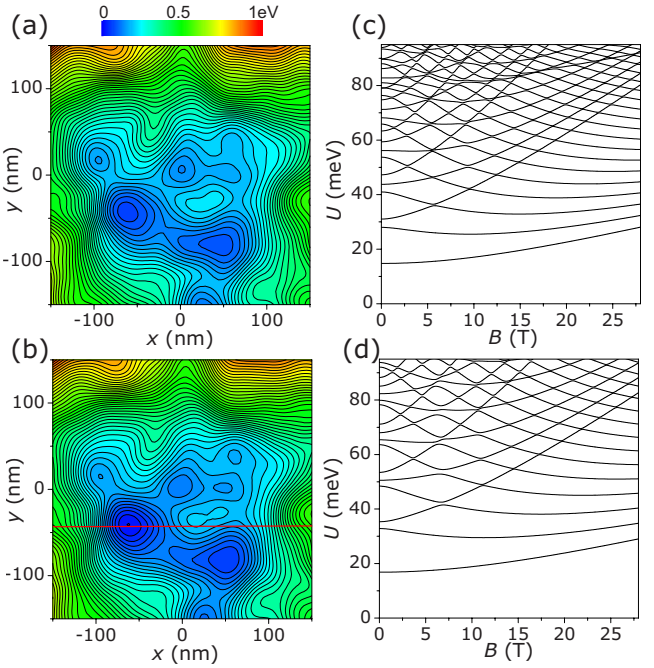

FIG. 4. (Color online) Numerical simulation of the electrostatic potential created by (a) a uniform "slab" and (b) a δ layer distribution of Mn_i donors. Parts (c) and (d) represent corresponding energy spectra of electrons confined in the potential minima.

III. NATURE OF THE POTENTIAL GENERATED BY RANDOMLY DISTRIBUTED CHARGES

We can gain further insight into the properties of the electrostatic potential induced by randomly distributed charges by considering the statistical characteristics of the potential. Since the appearance and qualitative properties of the potential do not depend on the distribution along z, we use a simplified analysis in which the potential arises from a large number of point charges, q, distributed randomly on the (x,y) plane. We follow an approach similar to that used in Ref. 22 to study charge-density fluctuations in metal-oxide-semiconductor devices and insulated-gate field-effect transistors. We consider n charged particles distributed among N atomic cells with equal probability. In our experiment the number of Mn_i ions is much smaller than the number of atoms in the crystal; hence we consider only the case $n \ll N$. In this limit, the distribution of charge across the plane obeys Poissonian statistics and the corresponding electrostatic potential $\phi(r,z)$ created by such a distribution of charge is given by

$$\frac{\partial^2 \phi(r,z)}{\partial r^2} + \frac{\partial^2 \phi(r,z)}{\partial z^2} = -\frac{q}{4\pi\varepsilon\varepsilon_0}\eta(r)\delta(z), \tag{2}$$

where $z=0$ corresponds to the plane of charges, $r=\sqrt{x^2+y^2}$, $\eta(r)$ represents a Poissonian white (uncorrelated) noise with mean value and variance equal to n/N, δ is the delta function, ε_0 is a vacuum permittivity and ε is relative permittivity of the material. A Fourier transform with respect to z yields the linear stochastic differential equation

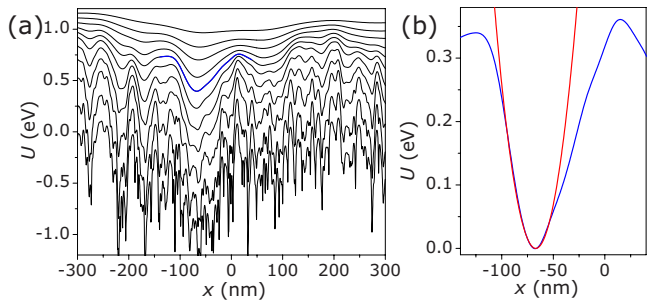

FIG. 5. (Color online) (a) Electrostatic potential profile along x for d=0.5, 1, 2, 4, 10, 15, 20, 30, 40, and 60 nm. For clarity the curves are shifted along the vertical axis. The thicker line, corresponding to d=15 nm, is shown in part (b) together with a parabolic fit around the minimum.

$$\frac{\partial^2\phi(r,k_z)}{\partial r^2} - k_z^2\phi(r,k_z) = -\frac{q}{4\pi\varepsilon\varepsilon_0}\eta(r), \tag{3}$$

which describes a stochastic process $\varphi(r,k_z)$, whose stationary autocorrelation function is $R(r',k_z)=\langle[\phi(r-r',k_z) - \langle\phi(r,k_z)\rangle][\phi(r,k_z)-\langle\phi(r,k_z)\rangle]\rangle \propto \exp(-k_z r')$. Here k_z is the spatial frequency along z and $\langle\cdot\rangle$ means averaging over the ensemble. One can formally introduce a correlation length r_c of the potential, which represents the distance r' at which $R(r',k_z)$ becomes e times smaller than its maximal value at $r'=0$, i.e., $r_c=1/k_z$. Thus, at distances $z=d\propto 1/k_z$ from the plane of charges at $z=0$, the potential has a longer correlation length across the (x,y) plane. In other words, Eq. (3) filters only large-scale fluctuations with higher spatial frequency. This conclusion is confirmed by the numerical simulation of $\phi(r,z)$ in Fig. 5(a), which shows that as d increases the potential becomes smoother.

To estimate the amplitude of the random fluctuations of the potential at a given distance, z, we assume that the charged particles are distributed homogeneously across the plane. The probability of finding a particle in a cell is $p=n/N$ and the mean value of the potential created by a single cell is $\langle\varphi_1\rangle=p\varphi_1$, where $\varphi_1=q(4\pi\varepsilon\varepsilon_0\sqrt{z^2+r^2})^{-1}$ is the potential generated by an individual charge at a distance $\sqrt{z^2+r^2}$. The corresponding mean-square deviation is $\sigma_1^2 = \langle(\varphi_1-\langle\varphi_1\rangle)^2\rangle = p\varphi_1^2$. For a cell of size a, the number of cells between r and $(r+dr)$ is $dN=2\pi r dr/a^2$. By integrating dN over all cells in the plane, we derive the mean-square fluctuation of the total potential

$$\sigma^2 = \int_0^R p\varphi_1^2\frac{2\pi r dr}{a^2} = \frac{pq^2}{8\pi(a\varepsilon\varepsilon_0)^2}\ln\left(1+\frac{R^2}{z^2}\right), \tag{4}$$

where R is the radius of the mesa. Equation (4) shows that the amplitude of the potential fluctuations goes to zero as z tends to infinity, as confirmed by our numerical simulations.

To understand qualitatively how a deep confining potential can be created, we consider a small number, n, of closely spaced positive electrical charges, q, placed at a small distance d above the origin of the (x,y) plane. The charges give rise to a confining potential $U(x,y)=-U_0/(1+r^2/d^2)^{1/2}$, where $U_0=nqe/(4\pi\varepsilon_0\varepsilon d)$ and $r^2=x^2+y^2$. Since the potential is approximately parabolic close to its minimum, i.e., $U(x,y)\sim -U_0(1-r^2/2d^2)$ [see also Fig. 5(b)], the low-lying two-dimensional eigenstates are simple harmonic-like, with an energy separation of $\hbar(U_0/m^*d^2)^{1/2}$ and characteristic length scale, ℓ_0, given by $\ell_0^2=d/(\hbar/m^*U_0)^{1/2}$, where m^* is the electron effective mass. Hence the depth and characteristic energy level spacing are determined by two parameters, n and d. If we assume that the potential can be approximated by a parabola up to an energy of $\approx U_0/2$, then the K lowest energy levels will approximate to those of an harmonic oscillator. Here $K=[\frac{1}{2}\frac{d}{\hbar}\sqrt{meU_0}]_I$, where $[\cdot]_I$ is the nearest integer function. Since $U_0\propto 1/d$, $K\propto\sqrt{d}$. For a nanocluster of 7 Mn_i ions placed at a distance d=18 nm, K=3, l_0=20 nm, and the principal level spacing is $\hbar\omega_0$=18 meV, in good agreement with the numerical results shown in Fig. 4 and the experimental data described below. Note that the spectrum of quantum-confined states of a potential minimum formed by a small cluster of donor ions outside the QW is quite different from those arising from δ doping with ionized donors in the plane of the QW. In the latter case, only the ground states of isolated 2D hydrogenic donors[23] and of "donor molecules"[24] can be observed by magnetotunneling spectroscopy; excited states are too close to the continuum to be resolved.

IV. EXPERIMENT AND DISCUSSION

We now consider the practical realization and electronic properties of nanoelectrostatic QDs and how the properties can be "tuned" in appropriately designed heterostructures. For these studies, we use the *p-i-n* RTD structures described in Sec. II. The *p-i-n* layers were grown by molecular-beam epitaxy and processed into circular mesas of diameter D =200 μm. By controlled annealing (T_A=150–200 °C and t_A=2–3 h), Mn interstitials ions were diffused out of the (GaMn)As layer into an adjacent layer of undoped GaAs. This creates a layer of randomly distributed, positively charged Mn_i^{2+} donors spatially separated from the (GaMn)As layer—as shown schematically in Fig. 1(d). The low-temperature (T=4.2 K) current-voltage characteristics, $I(V)$, of two separate mesa diodes are shown in Figs. 6(a) and 6(b). They both reveal sharp resonant peaks at applied voltages below the flat band condition. The resonances arise from electron tunneling from the n-type GaAs emitter into discrete QD states.

To probe the strength and symmetry of the QD confinement potential, we now examine the magnetotunneling spectra of these two mesas. Figures 6(c) and 6(d) shows gray scale plots of the intensity of the differential conductance dI/dV as a function of V and magnetic fields B (up to ~30 T) applied perpendicular to the plane of the QW. The dominant lines in each spectrum reveal a magnetic field dependence characteristic for the ground and excited states of a single quantum dot. For both gray scale plots, the lowest bias resonance reveals no Zeeman splitting, but a clear diamagnetic shift consistent with a ground-state orbital. We refer to the dots giving rise to the spectra in Figs. 6(a)–6(d) as QD1 and QD2, respectively. A striking difference between the two QDs is that the excited states of QD1 show a strong orbital Zeeman splitting, $\sim\hbar\omega_c$, remarkably similar to that of the Fock-Darwin model for a QD with circular symmetry[18] and

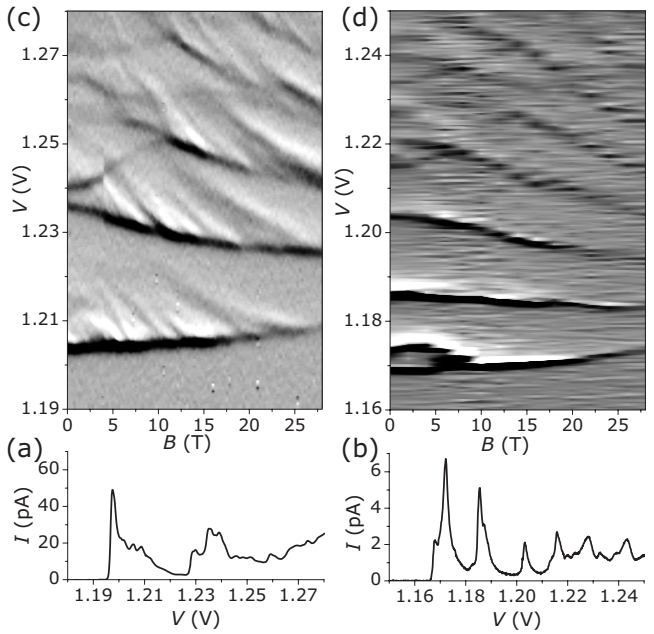

FIG. 6. (a) and (b) $I(V)$ at zero magnetic field (T=4.2 K) for two mesa diodes. The corresponding gray scale plots of the differential conductivity as a function of V and B parallel to z are shown in (c) and (d), respectively.

quantization energy $\hbar\omega_0 \sim 20$ meV. However, the small splitting at $B=0$ of the first two excited states ($2p_{x,y}$-like) in Fig. 6(c) indicates that QD1 does not have precise circular symmetry. A similar spectrum of levels is shown in Fig. 2(d) for a typical QD obtained in our simulation. In contrast, for QD2, we observe a series of four approximately equally spaced low-lying energy levels with no clear orbital Zeeman splitting. Their magnetic field dependence resembles that of one of the QDs found in our simulation, see Figs. 3(a) and 3(b), and reported for elongated QDs (Ref. 20) and wires[25] produced by submicron lithography. For the simulation presented in Figs. 3(a) and 3(b), the lowest energy states are equally separated by $\hbar\omega_0 \sim 20$ meV, which is the quantization energy for electron motion along the direction of weak confinement. We have measured the magnetotunneling spectra of 20 samples with quantum dots. Most of these dots have energy spectra similar to the Fock-Darwin model, thus indicating an approximately circular symmetric potential. Only two of the measured samples have energy spectra that indicate large deviations from circular symmetry. Figures 6(c) and 6(d) represent, respectively, these two types of behavior. Our observations are consistent with our statistical analysis of the shapes of the quantum dots generated by the random diffusion of Mn interstitials, see Fig. 3(c).

The good agreement between the analytical model, statistical and numerical analyses, and experimental results obtained in our (GaMn)As-based RTDs suggests that similar QD-like potentials could be created in other material systems and device structures. We have observed similar, though weaker, resonances in $I(V)$ curves of a second series of p-i-n QW RTDs. The molecular-beam epitaxy-grown epilayer, from which the diodes were produced, contained no Mn between the carbon-doped p GaAs and the QW, but a 10 nm layer of Si donors ($\sim 5\times 10^{18}$ cm^{-3}), which was intentionally introduced in the GaAs spacer layer at a distance of 15 nm from the central QW (x,y) plane. In these structures, the randomly distributed positive charges of the ionized substitutional Si^+ donors create a fluctuating potential with QD-like potential minima. These tend to be shallower than in the case of Mn-based structures due to the single positive (rather than double in Mn_i) charge of the Si ions.

We conclude this section by relating our results to some interesting reports of QD-like energy levels observed in device structures containing unintentional dopants or regions doped with Si dopants.[13–15] These papers have reported the observation of QDs with large ($\sim$10 meV) confinement energies. These have been attributed to "growth-induced" effects[13,14] or "fluctuations in the Si-donor concentration."[15] The magnetotunneling spectra presented in these papers resemble that of the Fock-Darwin model but with symmetry lowered by some unknown mechanism, possibly an ionized acceptor positioned at small distance away from the minimum of the approximately parabolic confinement potential. Our simulations confirm that the random character of the Coulomb potential generated by ionized impurities can indeed lead to deep, approximately parabolic and sometimes anisotropic confining potential minima. Such impurities can be intentionally introduced, as in our case, or exist in nominally undoped regions or at the interface of intentionally doped layers.

V. CONCLUSIONS

In conclusion, we have shown that randomly distributed charges placed close to a QW can produce deep and strongly confined quantum-dot-like potential minima with a rich spectrum of zero-dimensional energy levels. Since the potential is approximately parabolic close to its minima, the low-lying two-dimensional eigenstates are simple harmoniclike, with an energy separation and characteristic length scale determined by the number of charges and their distance from the well. Most of the deep potential minima have approximately circular symmetry, but a small number are significantly elongated to quench the orbital angular momentum. The high thermal diffusivity of ionized interstitial impurities such as doubly ionized manganese interstitial donors, Mn_i^{2+}, in GaAs, provides a means of realizing this type of nanoelectrostatic QD by controlled thermal annealing of appropriately designed heterostructures. On the other hand our calculations indicate that a similar result could be obtained for any random distribution of charges close to a QW.

ACKNOWLEDGMENTS

We thank the Engineering and Physical Sciences Research Council (U.K.) and the Royal Society (U.K.) for their support. The authors gratefully acknowledge discussions with A. Nikitin (University of Warwick, U.K.).

*Corresponding author.

[1] D. Bimberg, M. Grundmann, and N. N. Ledentsov, *Quantum Dot Heterostructures* (Wiley, New York, 1999), and references therein.
[2] J.-Y. Marzin, J.-M. Gérard, A. Izraël, D. Barrier, and G. Bastard, Phys. Rev. Lett. **73**, 716 (1994).
[3] R. J. Nötzel, J. Temmyo, and T. Tamamura, Nature (London) **369**, 131 (1994).
[4] L. Landin, M. S. Miller, M.-E. Pistol, C. E. Pryor, and L. Samuelson, Science **280**, 262 (1998).
[5] A. P. Alivisatos, Science **271**, 933 (1996).
[6] S. A. Empedocles and M. G. Bawendi, Science **278**, 2114 (1997).
[7] K. Tsutsui, E. L. Hu, and C. D. W. Wilkinson, Jpn. J. Appl. Phys., Part 1 **32**, 6233 (1993).
[8] K. Kash, A. Scherer, J. M. Worlock, H. G. Craighead, and M. Tamargo, Appl. Phys. Lett. **49**, 1043 (1986).
[9] A. Zrenner, L. V. Butov, M. Hagn, G. Abstreiter, G. Bohm, and G. Weimann, Phys. Rev. Lett. **72**, 3382 (1994).
[10] C. G. Smith, M. Pepper, H. Ahmed, J. E. F. Frost, D. G. Hasko, D. C. Peacock, D. A. Ritchie, and G. A. C. Jones, J. Phys. C **21**, L893 (1988).
[11] S. Tarucha, D. G. Austing, T. Honda, R. J. van der Hage, and L. P. Kouwenhoven, Phys. Rev. Lett. **77**, 3613 (1996).
[12] O. Makarovsky, O. Thomas, A. G. Balanov, L. Eaves, A. Patanè, R. P. Campion, C. T. Foxon, E. E. Vdovin, D. K. Maude, G. Kiesslich, and R. J. Airey, Phys. Rev. Lett. **101**, 226807 (2008).
[13] J. Könemann, R. J. Haug, D. K. Maude, V. I. Fal'ko, and B. L. Altshuler, Phys. Rev. Lett. **94**, 226404 (2005).
[14] E. Räsänen, J. Könemann, R. J. Haug, M. J. Puska, and R. M. Nieminen, Phys. Rev. B **70**, 115308 (2004).
[15] R. C. Ashoori, H. L. Stormer, J. S. Weiner, L. N. Pfeiffer, S. J. Pearton, K. W. Baldwin, and K. W. West, Phys. Rev. Lett. **68**, 3088 (1992).
[16] K. W. Edmonds, P. Boguslawski, K. Y. Wang, R. P. Campion, S. N. Novikov, N. R. S. Farley, B. L. Gallagher, C. T. Foxon, M. Sawicki, T. Dietl, M. Buongiorno Nardelli, and J. Bernholc, Phys. Rev. Lett. **92**, 037201 (2004).
[17] B. K. Ridley, Semicond. Sci. Technol. **3**, 286 (1988).
[18] S. M. Reimann and M. Manninen, Rev. Mod. Phys. **74**, 1283 (2002).
[19] R. C. Ashoori, H. L. Stormer, J. S. Weiner, L. N. Pfeiffer, K. W. Baldwin, and K. W. West, Phys. Rev. Lett. **71**, 613 (1993).
[20] D. G. Austing, S. Sasaki, S. Tarucha, S. M. Reimann, M. Koskinen, and M. Manninen, Phys. Rev. B **60**, 11514 (1999).
[21] J. A. Nixon and J. H. Davies, Phys. Rev. B **41**, 7929 (1990).
[22] J. R. Brews, J. Appl. Phys. **43**, 2306 (1972); **46**, 2181 (1975).
[23] J.-W. Sakai, T. M. Fromhold, P. H. Beton, L. Eaves, M. Henini, P. C. Main, F. W. Sheard, and G. Hill, Phys. Rev. B **48**, 5664 (1993).
[24] A. K. Geim, T. J. Foster, A. Nogaret, N. Mori, P. J. McDonnell, N. La Scala, Jr., P. C. Main, and L. Eaves, Phys. Rev. B **50**, 8074 (1994).
[25] P. H. Beton, J. Wang, N. Mori, L. Eaves, P. C. Main, T. J. Foster, and M. Henini, Phys. Rev. Lett. **75**, 1996 (1995).